Supporting Information

Thermal stability of Fe-Mn binary olivine cathode for Li rechargeable battery

Jongsoon Kim[1], *Kyu-Young Park*[2], *Inchul Park*[2], *Jung-Keun Yoo*[3], *Jihyun Hong*[1], *and Kisuk Kang*[1]*

[1]Department of Materials Science and Engineering, Seoul National University, 599 Gwanak-ro, Gwanak-gu, Seoul, Korea 151-742,

[2]Graduate school of Energy, Environment, Water and Sustainability (EEWS), [3]Department of Materials Science and Engineering, KAIST (Korea Advanced Institute of Science and Technology), Gwahangno 335, Yuseong-gu, Daejeon, Korea 305-701

Corresponding Author: Prof. Kisuk Kang

E-mail: matlgen1@snu.ac.kr

TEL: +82-2-880-7088

S1. As-prepared $LiFe_{1-x}Mn_xPO_4$ ($0 \leq x \leq 1$)

The XRD patterns of the as-prepared $LiFe_{1-x}Mn_xPO_4$ ($0 \leq x \leq 1$) are shown in Supporting Figure S1. Phase-pure olivine materials were identified from the powder XRD measurements. No noticeable impurity or second phase was observed in the XRD pattern of each sample. The solid solution between $LiMnPO_4$ and $LiFePO_4$ was confirmed at $0 \leq x \leq 1$ of $LiFe_{1-x}Mn_xPO_4$ with continuous variations in the lattice parameters *a*, *b*, and *c* as tabulated in Supporting Table S2.[1, 2] The small difference in lattice parameters among $LiFe_{1-x}Mn_xPO_4$ was caused by the different ionic radii of Mn^{2+} and Fe^{2+} ($Mn^{2+} > Fe^{2+}$) and their composition ratio in the materials.[3-5]

The thermal stability of the as-prepared $LiFe_{1-x}Mn_xPO_4$ series was first examined. Supporting Figure S2 shows the XRD patterns of each $LiFe_{1-x}Mn_xPO_4$ measured from 25°C to 700°C. No noticeable phase transformation was observed up to 700°C. Only the thermal expansion of the olivine crystal $LiFe_{1-x}Mn_xPO_4$ was detected from the shift of the XRD peaks at elevated temperatures. The quantitative analysis of the lattice parameter change from the Rietveld refinement is shown in Supporting Figure S3 with the thermal coefficients tabulated in Supporting Table S3. Linear thermal coefficients of *a*, *b*, and *c* lattices and the volumic thermal coefficients of the $Li_{1-y}Fe_{1-x}Mn_xPO_4$ samples were all within the same orders of magnitude.

The delithiated samples of $Li_{1-y}Fe_{1-x}Mn_xPO_4$ were prepared from the chemical method as described in the experimental section. It was observed that the delithiation process generally took longer with higher contents of Mn in the sample, which is in agreement with the fact that Mn-rich olivine cathodes usually exhibit a low power capability.[6] The delithiation mechanism of $Li_{1-y}Fe_{1-x}Mn_xPO_4$ at 25°C was monitored by the XRD patterns, as shown in Supporting Figure S4. Similar to previous reports,[7, 8] the delithiation mechanism of the two-phase reaction was observed with the single component olivine ($LiFePO_4$ and $LiMnPO_4$). However, the binary component olivine showed a mixed behavior of one-phase and two-phase reactions. Delithiation of $LiFe_{0.5}Mn_{0.5}PO_4$ and $LiFe_{0.25}Mn_{0.75}PO_4$ exhibited the growth of a new delithiated olivine phase accompanied with an apparent XRD peak shift of the mother phase ($LiFe_{0.5}Mn_{0.5}PO_4$ and $LiFe_{0.25}Mn_{0.75}PO_4$).[2] In the case of $LiFe_{0.75}Mn_{0.25}PO_4$, the XRD peaks were continuously shifted with delithiation and no emerging new XRD peaks from the second phases was observed. In the following sections, we evaluated the thermal characteristics of $Li_{1-y}Fe_{1-x}Mn_xPO_4$ using these prepared samples.

S2. *In-situ* XRD patterns of $Li_{1-y}Fe_{1-x}Mn_xPO_4$ ($0 \leq x, y \leq 1$)

Supporting Figure S5 shows that *in-situ* XRD patterns of fully delithiated $Fe_{1-x}Mn_xPO_4$ ($0 \leq x \leq 1$) at temperature from 25°C to 700°C and at 2θ from 15° to 45°. All fully delithiated phase experienced a two-tiered thermal decomposition by elevated temperatures. First, $Fe_{1-x}Mn_xPO_4$ ($0 \leq x \leq 1$) were decomposed into $(Fe_{1-x}Mn_x)_3(PO_4)_2$ ($0 \leq x \leq 1$). After more heating, $(Fe_{1-x}Mn_x)_3(PO_4)_2$ ($0 \leq x \leq 1$) were finally decomposed into $(Fe_{1-x}Mn_x)_2P_2O_7$ ($0 \leq x \leq 1$). The first decomposition temperature of each fully delithiated phase was influenced by Mn contents in the structure. Higher Mn contents exhibited poor thermal stability of the materials.

Supporting Figure S6 shows that *in-situ* XRD patterns of partially delithiated $Li_{1-y}Fe_{1-x}Mn_xPO_4$ ($0 \leq x \leq 1$, $y \approx 0.6$) at temperature from 25°C to 700°C and at 2θ from 15° to 45°. The XRD patterns of $Li_{0.6}FePO_4$, $LiFe_{0.5}Mn_{0.5}PO_4$, and $LiFe_{0.25}Mn_{0.75}PO_4$ started to merge with the appearance of broad patterns for the solid solution phase at high temperature (≥ 250°C) and $LiFe_{0.75}Mn_{0.25}PO_4$ exhibited the solid solution phase at room temperature. In case of $Li_{0.5}MnPO_4$, the fully delithiated phase (=$MnPO_4$) gradually disappeared and the

$Mn_3(PO_4)_2$ phase appeared at the expense of $MnPO_4$ instead of forming a solid solution of $Li_{0.5}MnPO_4$ as observed for $Li_{0.6}FePO_4$. At more elevated temperature ($\geq 550^oC$), all partially delithiated materials are decomposed into $Fe_{1-x}Mn_xP_2O_7$ ($0 \leq x \leq 1$, $y \approx 0.6$).

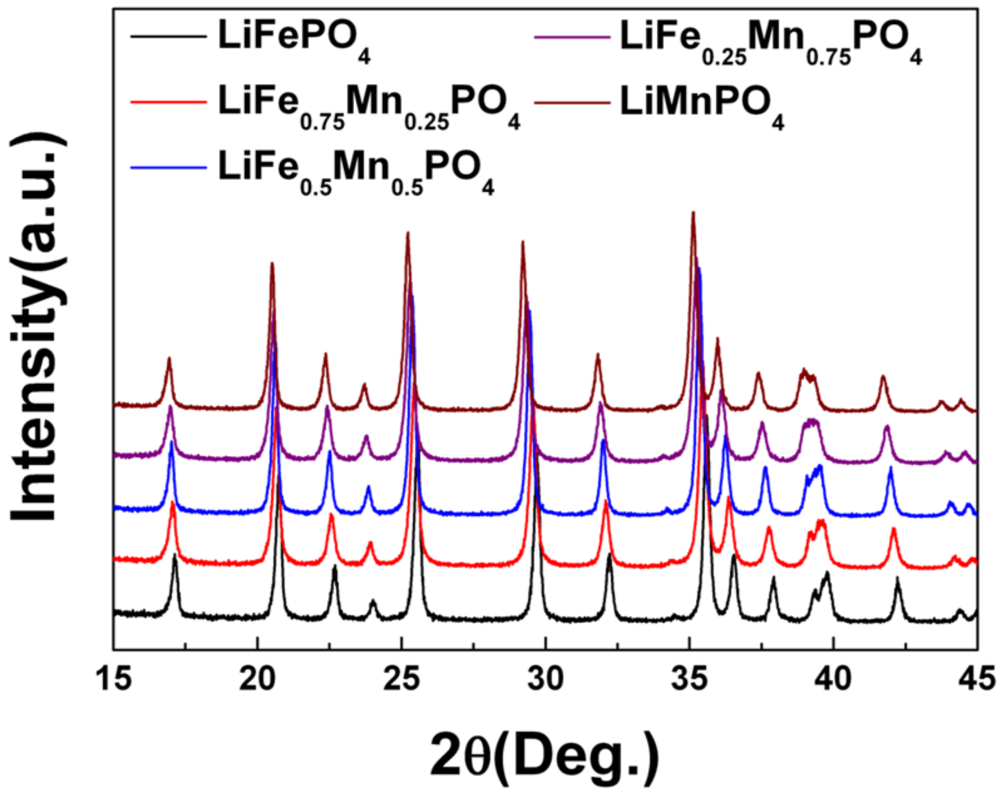

Figure S1 XRD patterns of as-prepared $LiFe_{1-x}Mn_xPO_4$ $[0 \leq x \leq 1]$

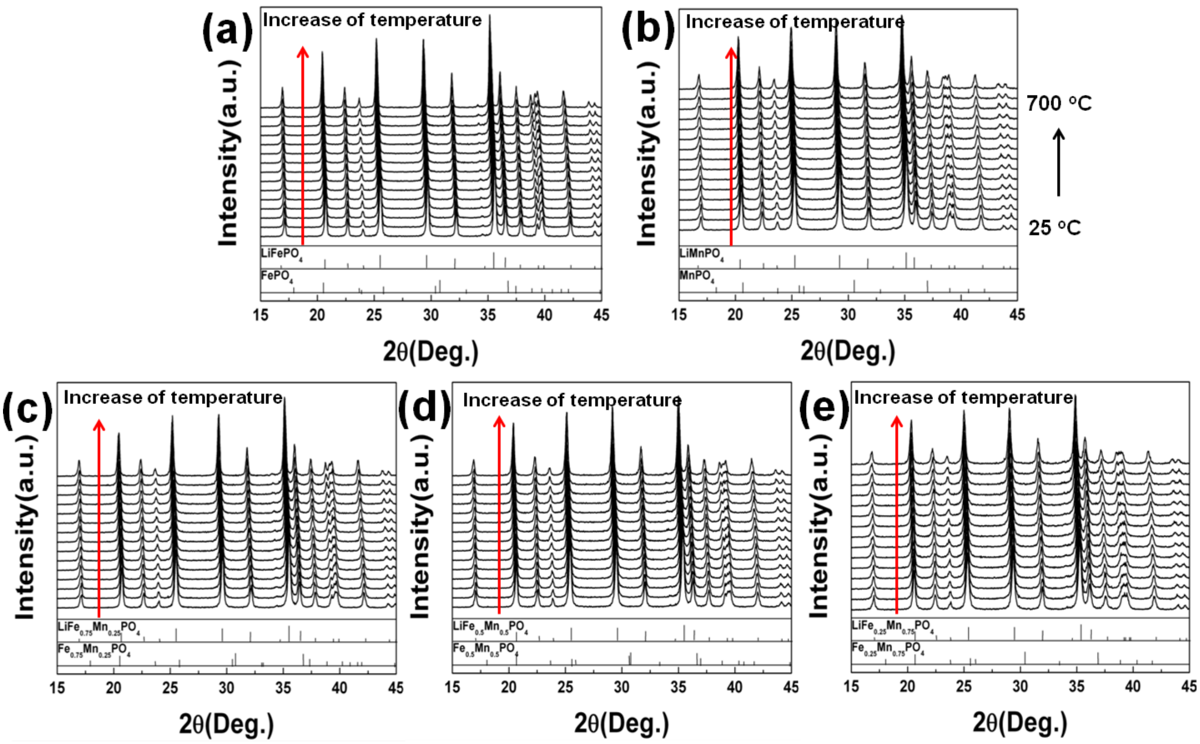

Figure S2 *in-situ* XRD patterns of as-prepared (a) $LiFePO_4$, (b) $LiMnPO_4$, (c) $LiFe_{0.75}Mn_{0.25}PO_4$, (d) $LiFe_{0.5}Mn_{025}PO_4$, and (e) $LiFe_{0.25}Mn_{0.75}PO_4$ at temperature from 25^{o}C to 700^{o}C and at 2θ from 15^o to 45^o

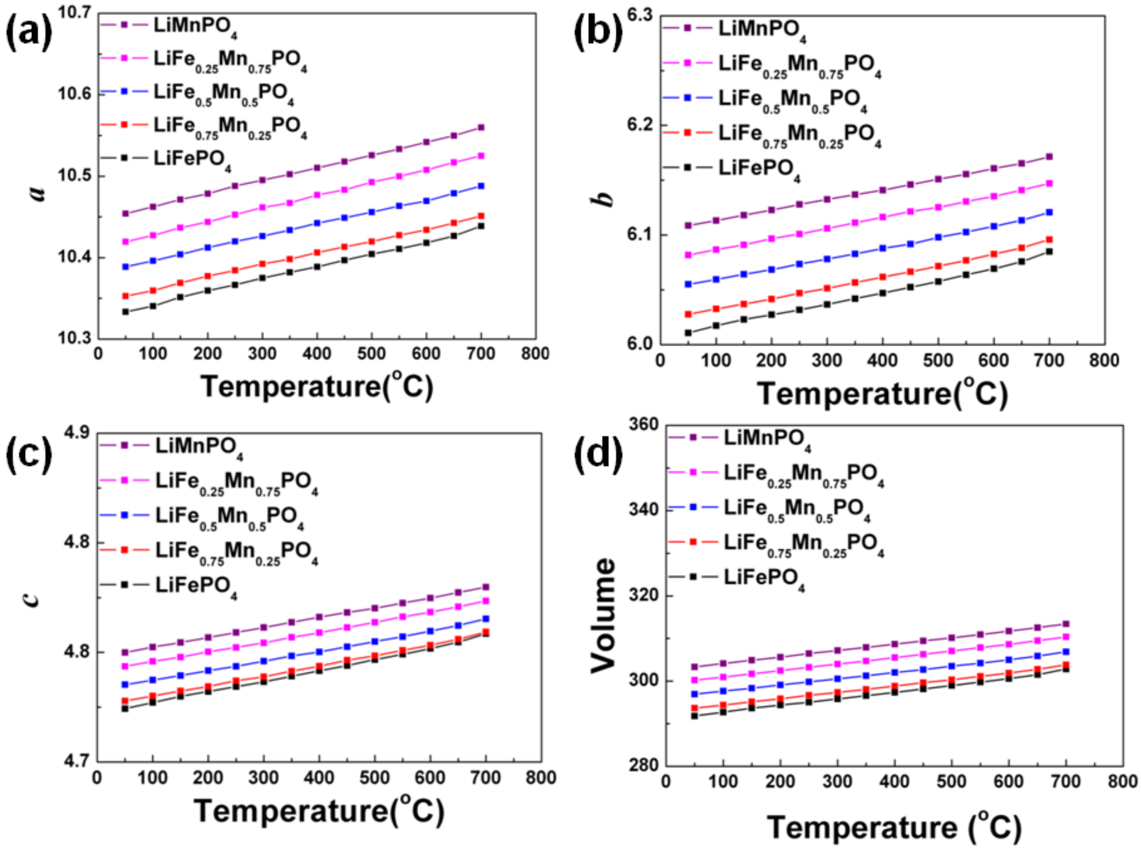

Figure S3 (a) Lattice parameter *a*, (b) Lattice parameter *b*, (c) Lattice parameter *c*, and (d) volume of $LiFe_{1-x}Mn_xPO_4$ [$0 \leq x \leq 1$] varied by temperature.

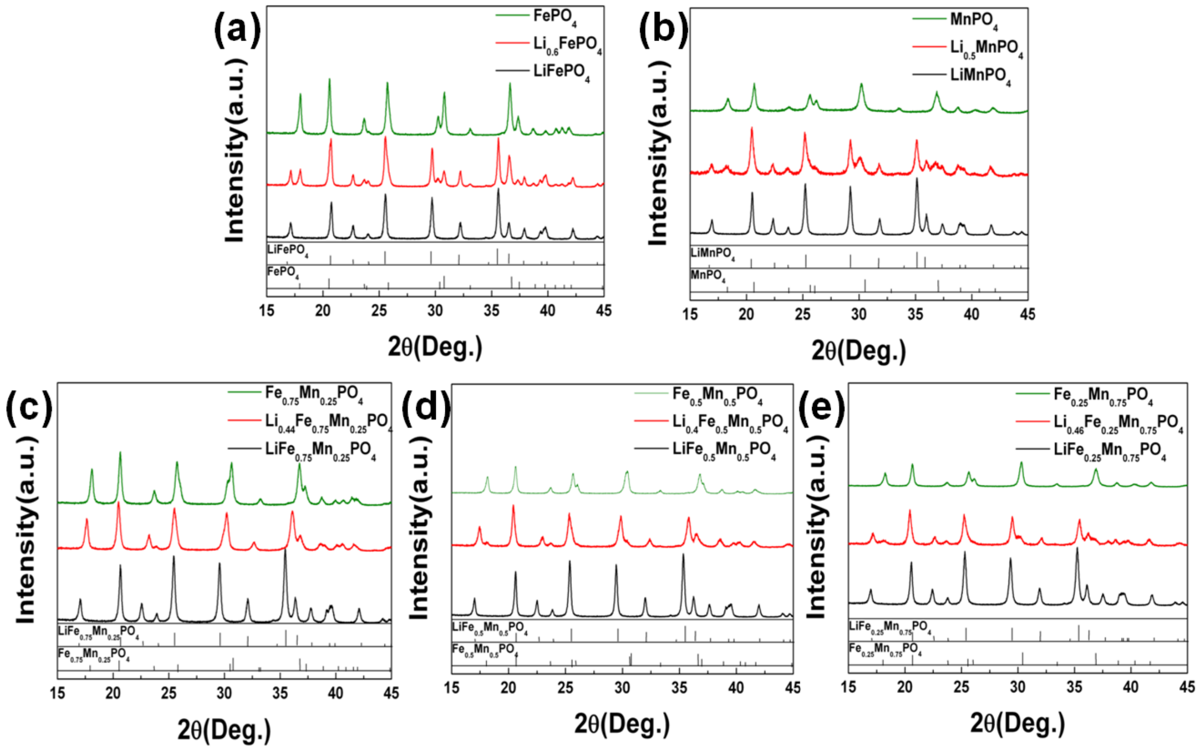

Figure S4 (a) Evolution of XRD patterns of (a) $Li_{1-y}FePO_4$ (b) $Li_{1-y}MnPO_4$, (c) $Li_{1-y}Fe_{0.75}Mn_{0.25}PO_4$, (d) $Li_{1-y}Fe_{0.5}Mn_{0.5}PO_4$, and (e) $Li_{1-y}Fe_{0.25}Mn_{0.75}PO_4$ [$0 \leq y \leq 1$] with a delithiation process.

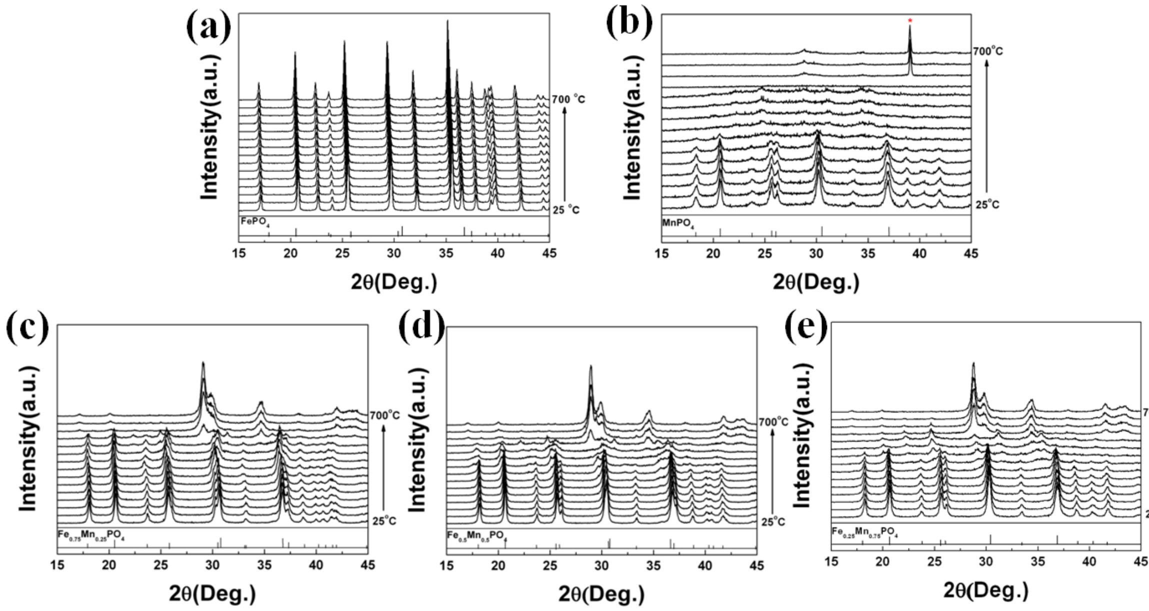

Figure S5 *in-situ* XRD patterns of fully delithiated (a) $FePO_4$, (b) $MnPO_4$ (* : the XRD peak of Pt holder), (c) $Fe_{0.75}Mn_{0.25}PO_4$, (d) $Fe_{0.5}Mn_{025}PO_4$, and (e) $Fe_{0.25}Mn_{0.75}PO_4$ at temperature from 25°C to 700°C and at 2θ from 15° to 45°

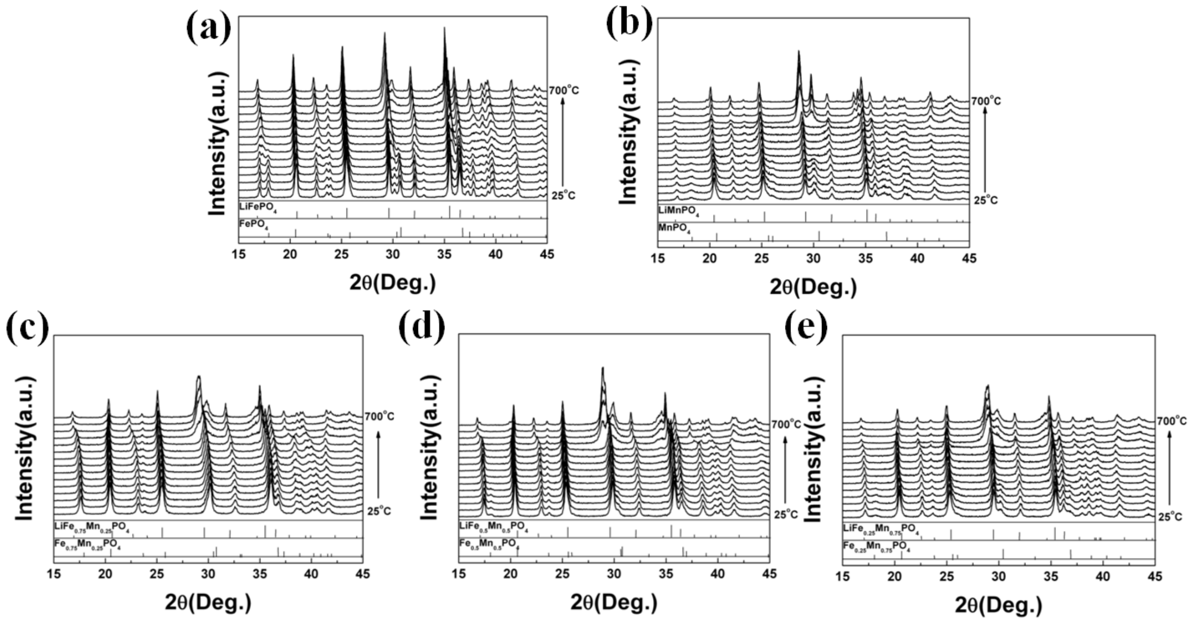

Figure S6 *in-situ* XRD patterns of partially delithiated (a) $Li_{0.6}FePO_4$, (b) $Li_{0.5}MnPO_4$, (c) $Li_{0.44}Fe_{0.75}Mn_{0.25}PO_4$, (d) $Li_{0.4}Fe_{0.5}Mn_{025}PO_4$, and (e) $Li_{0.46}Fe_{0.25}Mn_{0.75}PO_4$ at temperature from 25°C to 700°C and at 2θ from 15° to 45°

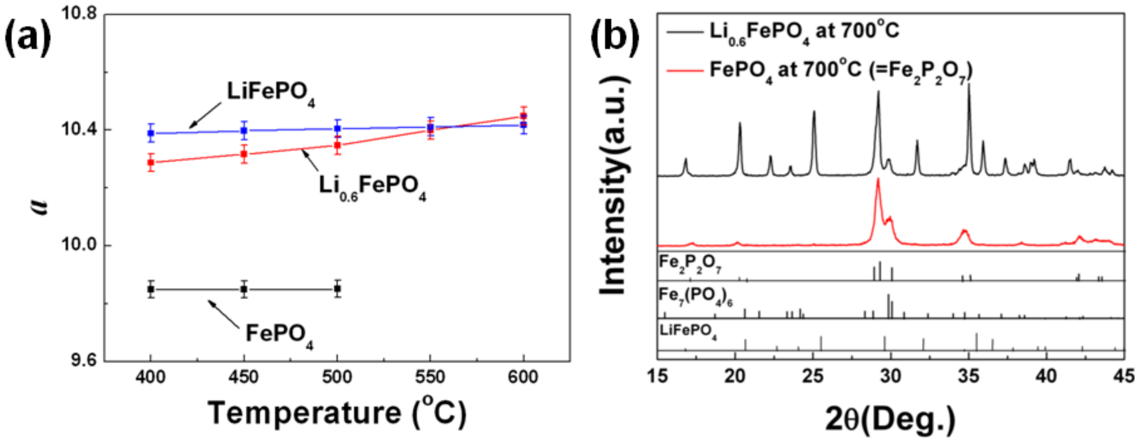

Figure S7 (a) Comparison of lattice parameter *a* of Li_yFePO_4 [y = 0, 0.6, and 1] varied by temperature and (b) XRD patterns of partially delithiated $Li_{0.6}FePO_4$ at 700°C compared with $Fe_2P_2O_7$ and $Fe_7(PO_4)_6$ among at 2θ from 15° to 45°.

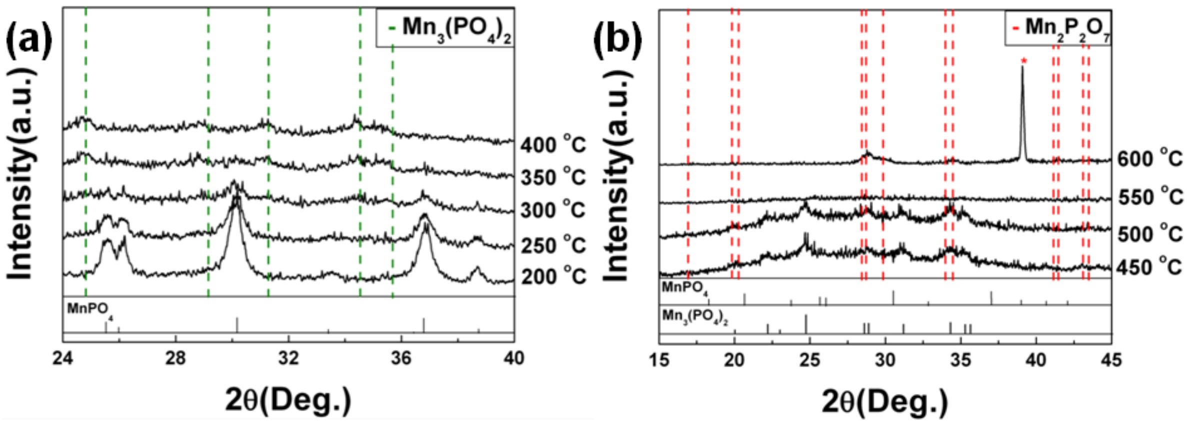

Figure S8 (a) *in-situ* XRD patterns of fully delithiated $MnPO_4$ at temperature from 200°C to 400°C and at 2θ from 24° to 40° and (b) *in-situ* XRD patterns of fully delithiated $MnPO_4$ at temperature from 450°C to 600°C and at 2θ from 15° to 45° (* : the XRD peak of Pt holder)

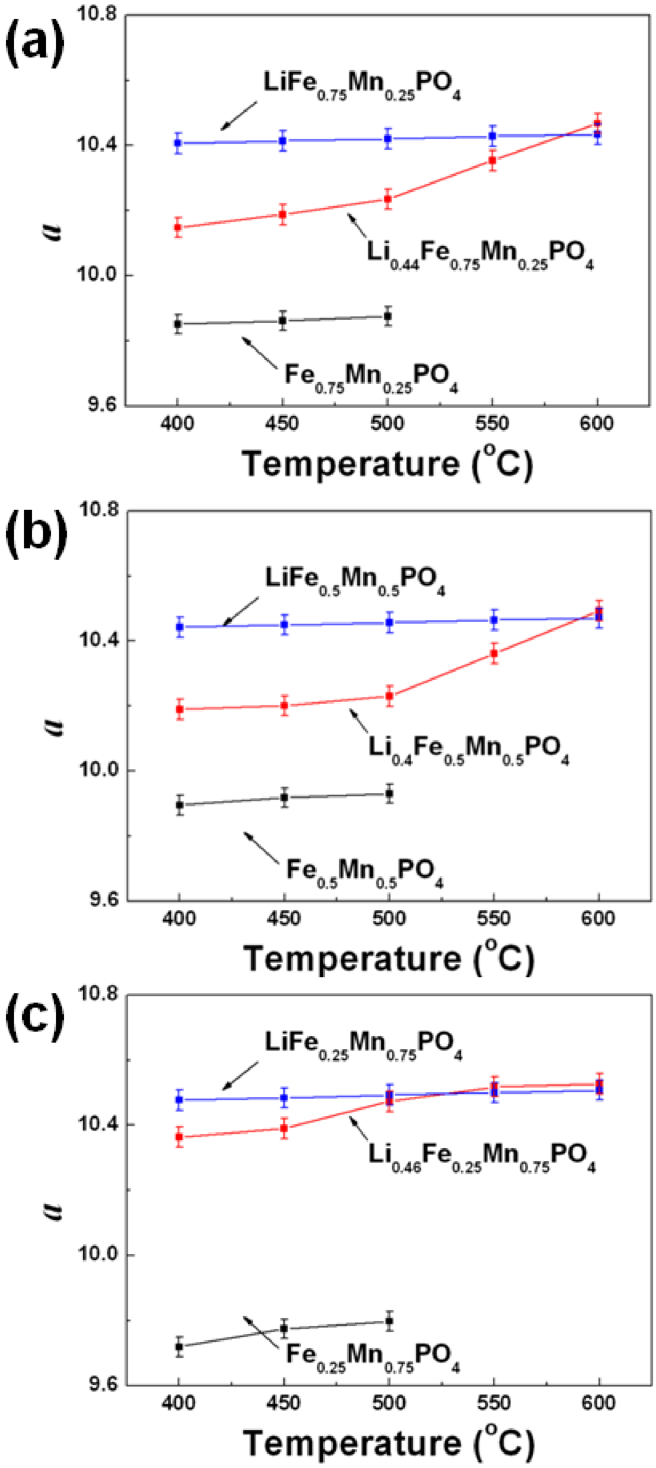

Figure S9 Comparison of lattice parameter *a* of (a) $Li_yFe_{0.75}Mn_{0.25}PO_4$ [y = 0, 0.44, and 1], (b) $Li_yFe_{0.5}Mn_{0.5}PO_4$ [y = 0, 0.4, and 1], and (c) $Li_yFe_{0.25}Mn_{0.75}PO_4$ [y = 0, 0.46, and 1] varied by temperature

	Atom	As-prepared phase	Partially delithiated phase	Fully delithiated phase
$Li_{1-y}FePO_4$	Li	1	0.6	0
	Fe	1	1	1
$Li_{1-y}Fe_{0.75}Mn_{0.25}PO_4$	Li	1	0.44	0
	Fe	0.75	0.75	0.75
	Mn	0.25	0.25	0.25
$Li_{1-y}Fe_{0.5}Mn_{0.5}PO_4$	Li	1	0.4	0
	Fe	0.5	0.5	0.5
	Mn	0.5	0.5	0.5
$Li_{1-y}Fe_{0.25}Mn_{0.75}PO_4$	Li	1	0.46	0
	Fe	0.25	0.25	0.25
	Mn	0.75	0.75	0.75
$Li_{1-y}MnPO_4$	Li	1	0.5	0
	Mn	1	1	1

Table S1 Atomic ratio of Li, Fe, and Mn in $Li_{1-y}Fe_{1-x}Mn_xPO_4$ $[0 \le x, y \le 1]$

	a (Å)	b (Å)	c (Å)
$LiFePO_4$	10.328	6.009	4.697
$LiFe_{0.75}Mn_{0.25}PO_4$	10.348	6.026	4.704
$LiFe_{0.5}Mn_{0.5}PO_4$	10.384	6.053	4.718
$LiFe_{0.25}Mn_{0.75}PO_4$	10.415	6.079	4.735
$LiMnPO_4$	10.450	6.106	4.748

Table S2 Lattice parameters of fully lithiated $LiFe_{1-x}Mn_xPO_4$ $[0 \leq x \leq 1]$

	Lattice	Thermal coefficient (K^{-1})
$LiFePO_4$	*a*	1.57×10^{-4}
	b	1.08×10^{-4}
	c	1.01×10^{-4}
	Volume	1.61×10^{-2}
$LiFe_{0.75}Mn_{0.25}PO_4$	*a*	1.49×10^{-4}
	b	1.02×10^{-4}
	c	9.49×10^{-5}
	Volume	1.53×10^{-2}
$LiFe_{0.5}Mn_{0.5}PO_4$	*a*	1.50×10^{-4}
	b	9.88×10^{-5}
	c	9.09×10^{-5}
	Volume	1.50×10^{-2}
$LiFe_{0.25}Mn_{0.75}PO_4$	*a*	1.61×10^{-4}
	b	9.90×10^{-5}
	c	9.07×10^{-5}
	Volume	1.55×10^{-2}
$LiMnPO_4$	*a*	1.59×10^{-4}
	b	9.49×10^{-4}
	c	9.09×10^{-5}
	Volume	1.53×10^{-2}

Table S3 The thermal coefficients of fully lithiated $LiFe_{1-x}Mn_xPO_4$ $[0 \leq x \leq 1]$

Reference

1. A. Yamada, Y. Takei, H. Koizumi, N. Sonoyama, R. Kanno, K. Itoh, M. Yonemura and T. Kamiyama, *Chem. Mat.*, 2006, **18**, 804-813.
2. A. Yamada, Y. Kudo and K. Y. Liu, *J. Electrochem. Soc.*, 2001, **148**, A1153-A1158.
3. R. D. Shannon and C. T. Prewitt, *Acta Cryst.B*, 1969, **B 25**, 925-&.
4. D. H. Seo, H. Gwon, S. W. Kim, J. Kim and K. Kang, *Chem. Mat.*, 2010, **22**, 518-523.
5. Y.-U. Park, J. Kim, H. Gwon, D. H. Seo, S. W. Kim and K. Kang, *Chem. Mat.*, 2010, **22**, 2573.
6. C. Delacourt, L. Laffont, R. Bouchet, C. Wurm, J. B. Leriche, M. Morcrette, J. M. Tarascon and C. Masquelier, *J. Electrochem. Soc.*, 2005, **152**, A913-A921.
7. S.-W. Kim, J. Kim, H. Gwon and K. Kang, *J. Electrochem. Soc.*, 2009, **156**, A635-A638.
8. C. Delacourt, P. Poizot, J.-M. Tarascon and C. Masquelier, *Nat Mater*, 2005, **4**, 254-260.